

A New Transition Wolf-Rayet WN/C Star in the Milky Way

WEI ZHANG,¹ HELGE TODT,² HONG WU,¹ JIANRONG SHI,¹ CHIH-HAO HSIA,³ YUZHONG WU,¹ CHAOJIAN WU,¹
YONGHENG ZHAO,¹ TIANMENG ZHANG,¹ AND YONGHUI HOU^{4,5}

¹*CAS Key Laboratory of Optical Astronomy, National Astronomical Observatories, Chinese Academy of Sciences, Beijing 100101, People's Republic of China*

²*Institut für Physik und Astronomie, Universität Potsdam, Karl-Liebknecht-Str. 24/25, 14476 Potsdam, Germany*

³*State Key Laboratory of Lunar and Planetary Sciences, Macau University of Science and Technology, Taipa, Macau, People's Republic of China*

⁴*University of Chinese Academy of Sciences, Beijing 100049, People's Republic of China*

⁵*Nanjing Institute of Astronomical Optics, & Technology, National Astronomical Observatories, Chinese Academy of Sciences, Nanjing 210042, People's Republic of China*

ABSTRACT

We report the discovery of a new transition type Wolf-Rayet (WR) WN/C star in the Galaxy. According to its coordinates (R.A., Dec)_{J2000} = 18^h51^m39^s.7, −05°34′51″.1, and the distance (7.11^{+1.56}_{−1.22} kpc away from Earth) inferred from the second *Gaia* data release, it's found that WR 121-16 is located in the Far 3kpc Arm, and it is 3.75 kpc away from the Galactic Center. The optical spectra obtained by the Large Sky Area Multi-Object Fiber Spectroscopic Telescope (LAMOST) and the 2.16 m telescope, both located at the Xinglong Observatory in China, indicate that this is a WR star of the transitional WN7o/WC subtype. A current stellar mass of about 7.1^{+1.7}_{−1.1} M_⊙, a mass-loss rate of $\dot{M} = 10^{-4.97^{+0.16}_{-0.20}}$ M_⊙ yr^{−1}, a bolometric luminosity of log $L/L_{\odot} = 4.88^{+0.17}_{-0.15}$, and a stellar temperature of $T_{*} = 47^{+9}_{-5}$ kK are derived, by fitting the observed spectrum with a specific Potsdam Wolf-Rayet (PoWR) model. The magnitude in *V*-band varies between 13.95 and 14.14 mag, while no period is found. Based on the optical spectra, the time domain data, and the indices of the astrometric solution of the *Gaia* data, WR 121-16 is likely a transitional WN/C single star rather than a WN+WC binary.

Keywords: stars: Wolf-Rayet – stars: massive – stars: distances – Galaxy: stellar content

1. INTRODUCTION

Wolf-Rayet (WR) stars are evolved descendants of the massive O stars with initial mass $M_i \gtrsim 25 M_{\odot}$. Unlike most stars whose spectra show narrow absorption lines, the WR stars have spectacular spectra with strong and broad emission lines, which are formed in the optically thick and extremely fast stellar winds (e.g., Crowther 2007). With a high mass-loss rate ($\sim 10^{-5} - 10^{-4} M_{\odot} \text{yr}^{-1}$) and ending their lives as core-collapse supernovae, they play an important role in shaping the structure and chemical evolution of their host galaxies. WR stars can also be progenitors of long-duration gamma-ray bursts (Callingham et al. 2019). The number of WR stars in the Milky Way is expected to be 1200 ± 200 (Rosslowe & Crowther

2015a,b). Even with the help of infrared observations which are suitable to detect obscured targets (Hillier et al. 1983; Hillier 1985; Crowther & Smith 1996; Roman-Lopes et al. 2020), only 666 WR stars have been found to date¹, indicating that about half of them are still hidden in the Galaxy.

According to the strong emission lines, WR stars can be classified as WN (helium and nitrogen), WC and WO (helium, carbon and oxygen) types. WN stars are believed to show the hydrogen burning products via the CNO cycle, while WC stars reveal the helium burning products via the triple- α cycle. Based on the strength of the emission lines and line ratios, WN stars can be further classified into the spectral subtypes WN2 to WN11, and WC stars into the spectral subtypes WC4 to WC9 (Smith 1968; Smith et al. 1990, 1994, 1996; Crowther et al. 1998). Also, there are transi-

Corresponding author: Wei Zhang
xtwfn@bao.ac.cn

¹ <http://pacrowther.staff.shef.ac.uk/WRcat/index.php>, v1.24

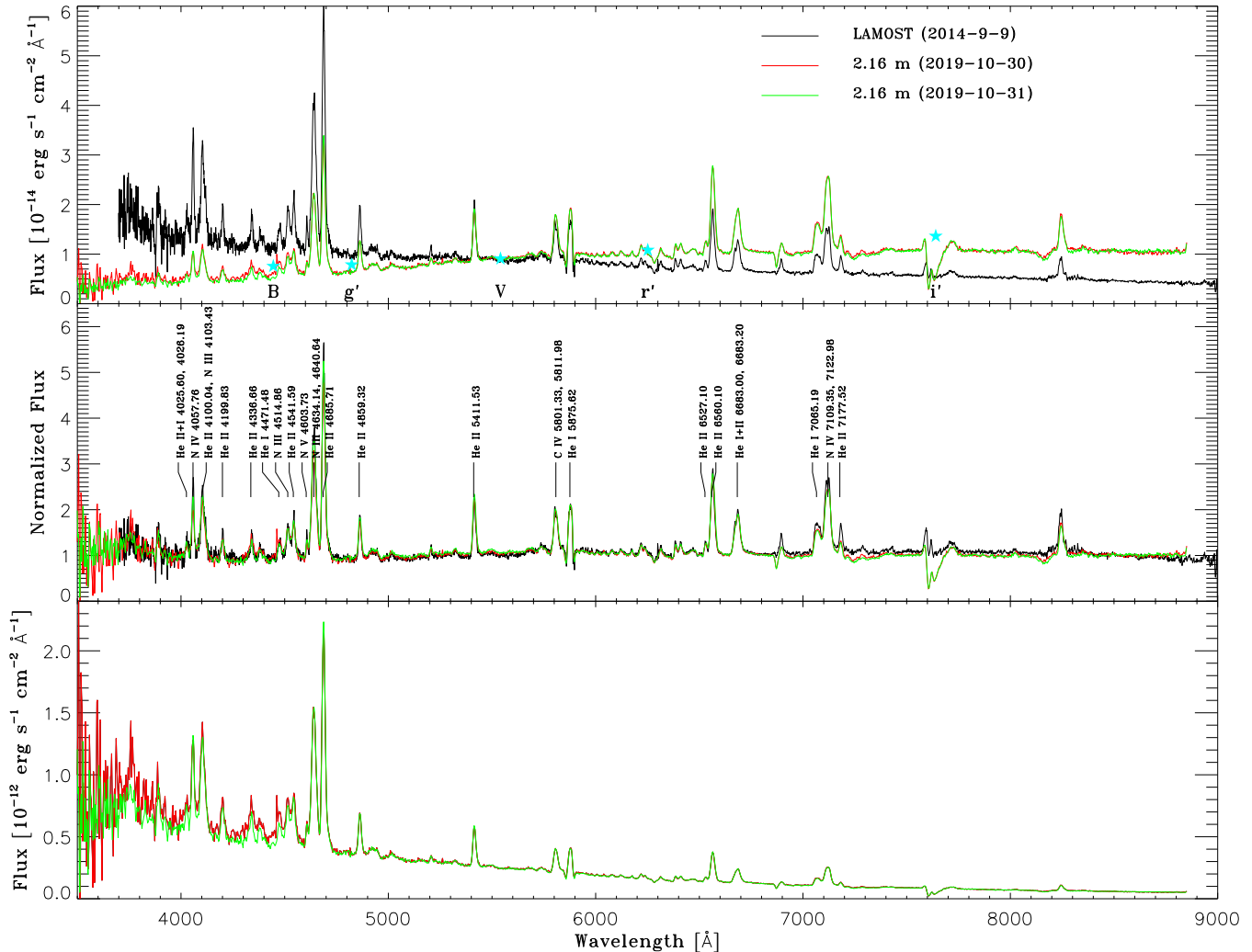


Figure 1. The observed spectra obtained at the LAMOST (black lines) and the 2.16 m telescope (red and green lines). In the top panel, the LAMOST spectrum has been shifted to a visual V magnitude of 14.024. The SED is shown as cyan filled stars. These three continuum normalized spectra with some line identifications are shown in the middle panel. The dereddened 2.16 m spectra are shown in the bottom panel. [The data of the three spectra are available in the electronic edition of the Journal.]

tion types from WN to WC, which are called WN/C or WC/N stars, whose spectra show strong emission lines of carbon and nitrogen simultaneously (Massey & Grove 1989; Conti & Massey 1989; Crowther 2007). As the duration of this transition phase is very short (~ 1 Myr), they are hard to find (Crowther et al. 1995). Only about a dozen of transition type stars are currently known in the Milky Way, the LMC, the SMC, IC10, NGC 1313, M31, M33 and M81 (Morgan & Good 1987; Conti & Massey 1989; Schild et al. 1990; Breysacher et al. 1999; Crowther et al. 2003; Hadfield & Crowther 2007; Massey et al. 2014; Shara et al. 2016; Gómez-González et al. 2016). We note that no WN/C star in M31 has been known to us until the first one was detected by Shara et al. (2016).

Having a large field of view (5° in diameter) and taking 4000 spectra in a single exposure, the Large Sky Area Multi-Object Fiber Spectroscopic Telescope (LAMOST) at the Xinglong Observatory in China is powerful to search for such rare objects. The strong emission lines of our target can be easily identified in the low-resolution spectrum ($R \sim 1800$), which covers the full optical range from 3700 to 9000 Å (Wang et al. 1996; Su & Cui 2004; Cui et al. 2012; Zhao et al. 2012; Luo et al. 2015). We here report a new WN/C star serendipitously discovered during the LAMOST testing observations carried out in the full moon nights.

The paper is structured as follows. In Section 2, we describe the observation and reduction of the optical spectra, and the spectral classification of the newly dis-

Table 1. The SED of the new WN/C star.

| Filters | Catalog | frequency (GHZ) | mag | mag err | magtype | Δmag^a |
|---------|---------|-----------------|--------|---------|---------|----------------------|
| B | APASS9 | 674.90e+3 | 14.819 | 0.017 | Vega | -0.163 |
| V | APASS9 | 541.43e+3 | 14.024 | — | Vega | -0.044 |
| g' | APASS9 | 621.98e+3 | 14.436 | — | asinh | 0.000 |
| r' | APASS9 | 479.90e+3 | 13.528 | — | asinh | 0.000 |
| i' | APASS9 | 392.66e+3 | 12.840 | 0.033 | asinh | 0.000 |
| J | 2MASS | 241.96e+3 | 11.369 | 0.032 | Vega | 0.910 |
| H | 2MASS | 181.75e+3 | 10.997 | 0.022 | Vega | 1.380 |
| Ks | 2MASS | 138.55e+3 | 10.609 | 0.019 | Vega | 1.850 |
| W1 | WISE | 89.490e+3 | 9.845 | 0.137 | Vega | 2.699 |
| W2 | WISE | 65.172e+3 | 9.747 | 0.115 | Vega | 3.339 |
| W3 | WISE | 25.934e+3 | 8.562 | 0.139 | Vega | 5.174 |
| W4 | WISE | 13.571e+3 | 7.505 | 0.161 | Vega | 6.620 |

NOTE— ^a $\text{mag}(\text{AB}) = \text{mag} + \Delta\text{mag}$

covered WR star. The stellar parameters are given in Section 3. We discuss the probability of the new WR star being a binary in Section 4, and summarize our results in Section 5.

2. DATA OBSERVATION AND ANALYSIS

2.1. Optical Spectra

The WR star discussed in this paper was found as a ‘by-product’ of the LAMOST testing observations during the full moon nights, when the telescope was pointing to the open cluster M11. The equatorial and galactic coordinates of this object are (R.A., Dec) = (18^h51^m39^s.7, −05°34′51″.1) and (l , b) = (01^h51^m56^s.9, −02°35′28″.0), respectively, which is about 42′.24 apart from the center of M11. Following the revised nomenclature scheme introduced in Appendix A of Rosslowe & Crowther (2015a) for Galactic WR stars, we name it WR 121-16. The visual magnitude in V -band for this star is 14.0, and the spectral energy distribution (SED) from the optical to the infrared is summarized in Table 1. The spectrum obtained on September 9, 2014, with an exposure time of 1800 s, is shown in the top panel of Figure 1 (black line). The data was reduced using the standard pipeline, including bias subtraction, flat correction, spectra extraction, wavelength calibration, and flux calibration (Luo et al. 2015). This low-resolution ($R \sim 1800$) spectrum shows strong nitrogen lines, such as N III $\lambda 4634$ - $\lambda 4641$ blend, N IV $\lambda 4057$, $\lambda 7109$, $\lambda 7123$. The N V $\lambda 4604$, $\lambda 4933$ - $\lambda 4944$ blend lines are relatively weak but can be clearly detected. The N V $\lambda 4620$ line is weak and blended to $\lambda 4634$ - $\lambda 4641$ blend lines. The He I and He II lines are also strong. The C IV $\lambda 5808$ line is strong, while C III $\lambda 5696$ line can not be detected.

We also carried out the followup observations using the BAO Faint Object Spectrograph and Camera

(BFOSC) on the 2.16 m telescope at the Xinglong Observatory in China on October 30 and 31, 2019, with an exposure time of 1200 s on each night (Zhao et al. 2018). The grating 300 l mm^{−1}, blazed at 6000 Å, and a slit width of 2.″0 was used and provided spectral coverage roughly from 3250 to 8850 Å with a resolving power $R \sim 1600$. The data was reduced using standard IRAF procedures, and the spectra are absolutely flux-calibrated using the standard star HR 7596, which was observed in the same night with an exposure time of 5 s. These two spectra (red and blue lines) have been compared with the LAMOST spectrum (black line) in Figure 1. In the top panel, the LAMOST spectrum has been shifted to $V = 14.024$ mag to make a comparison with the 2.16 m spectra. We can see that the 2.16 m spectra are identical with each other, while they have quite different slopes of the continuum compared to that one of the LAMOST spectrum. As the 2.16 m spectra have been absolutely flux-calibrated, we then compare them with the observed SED which is summarized Table 1. Note that the SDSS asinh magnitudes in g' , r' and i' -band are close to the AB system, while the Vega magnitudes should be converted to the AB system by adding the offsets Δmag listed in the last column of Table 1, and the data of Δmag are from Frei & Gunn (1994), Blanton & Roweis (2007) and Jarrett et al. (2011). It is found that the 2.16 m spectra are consistent with the SED shown as cyan stars. Hereafter, it tell us that there was some problem with the relative flux calibration for the LAMOST observation. This result is not strange for the large field of view and multi-fiber observations in the direction of high extinction regions. We have normalized all the three spectra and present them in the middle panel of Figure 1. We can see the line strengths of the LAMOST spectrum are now almost identical with those of the 2.16 m spectra.

We have measured the most prominent emission features, including the observed central wavelength, full width at half maximum (FWHM), flux and equivalent width (EW), and listed the results in Table 2. We should note that the flux of the LAMOST spectrum is not listed in this table. Moreover, as the spectra are affected by strong reddening (see Section 3.2), the measured fluxes from the original fluxed spectra may not represent the star properties. We then also measured the fluxes from the dereddened spectra (see the bottom panel of Figure 1) and listed them below the original ones. From this table, we can see that these lines do not change with time, as shown in the middle panel of Figure 1.

Table 2. Observational properties of the prominent emission lines. Flux is in units of 10^{-14} erg s $^{-1}$ cm $^{-2}$. For each emission line, the first row lists measurement results from the original fluxed spectrum, while the second row lists that from the dereddened one.

| Line Name | LAMOST (2014-9-9) | | | | 2.16 m (2019-10-30) | | | | 2.16 m (2019-10-31) | | | |
|------------------------------|-------------------|-------------|----------|-------------|---------------------|--------------|---------------|-------------|---------------------|-------------|---------------|-------------|
| | Wave | FWHM | Flux | EW | Wave | FWHM | Flux | EW | Wave | FWHM | Flux | EW |
| | (Å) | (Å) | (a) | (Å) | (Å) | (Å) | (a) | (Å) | (Å) | (Å) | (a) | (Å) |
| He II+I 4025.60, 4026.19 | 4028.85 ± 4.35 | 11.3 ± 10.8 | – | 4.6 ± 4.2 | 4026.56 ± 64.04 | 30.7 ± 193.0 | 4.1 ± 27.3 | 8.7 ± 58.0 | 4027.22 ± 27.02 | 12.2 ± 68.2 | 1.9 ± 10.6 | 4.3 ± 23.8 |
| | | | | | 4026.37 ± 0.52 | 32.1 ± 1.6 | 547.1 ± 29.5 | 9.2 ± 0.5 | 4027.19 ± 0.21 | 12.2 ± 0.5 | 246.2 ± 10.6 | 4.3 ± 0.2 |
| N IV 4057.76 | 4058.32 ± 1.02 | 10.4 ± 2.5 | – | 17.5 ± 4.0 | 4057.93 ± 10.44 | 15.9 ± 24.1 | 9.3 ± 15.1 | 19.3 ± 31.3 | 4058.03 ± 7.40 | 15.1 ± 18.6 | 9.7 ± 11.9 | 21.4 ± 26.3 |
| | | | | | 4057.91 ± 0.08 | 15.9 ± 0.2 | 1149.7 ± 15.5 | 19.3 ± 0.3 | 4057.99 ± 0.06 | 15.1 ± 0.2 | 1196.9 ± 11.9 | 21.3 ± 0.2 |
| He II 4100.04, N III 4103.43 | 4105.53 ± 1.93 | 23.2 ± 5.3 | – | 31.3 ± 7.8 | 4103.47 ± 9.80 | 26.5 ± 27.9 | 17.4 ± 20.9 | 34.8 ± 41.9 | 4104.58 ± 10.17 | 26.6 ± 29.2 | 16.7 ± 21.1 | 36.0 ± 45.4 |
| | | | | | 4103.33 ± 0.08 | 26.6 ± 0.2 | 2065.4 ± 21.1 | 35.0 ± 0.4 | 4104.45 ± 0.09 | 26.5 ± 0.2 | 1976.7 ± 21.0 | 35.8 ± 0.4 |
| He II 4199.83 | 4201.34 ± 2.94 | 9.5 ± 7.2 | – | 5.8 ± 4.1 | 4200.59 ± 19.15 | 17.3 ± 48.8 | 4.6 ± 13.2 | 9.4 ± 26.8 | 4201.55 ± 21.04 | 17.5 ± 53.7 | 4.3 ± 13.3 | 9.5 ± 29.3 |
| | | | | | 4200.53 ± 0.18 | 17.2 ± 0.5 | 498.9 ± 13.1 | 9.4 ± 0.2 | 4201.50 ± 0.19 | 17.5 ± 0.5 | 464.4 ± 13.3 | 9.5 ± 0.3 |
| He II 4336.66 | 4341.65 ± 3.70 | 11.7 ± 9.2 | – | 6.9 ± 5.2 | 4340.35 ± 25.74 | 23.5 ± 65.8 | 6.3 ± 17.9 | 11.2 ± 32.0 | 4339.15 ± 24.39 | 20.0 ± 63.5 | 4.5 ± 14.9 | 9.2 ± 30.3 |
| | | | | | 4340.25 ± 0.27 | 23.5 ± 0.7 | 586.2 ± 17.8 | 11.1 ± 0.3 | 4339.06 ± 0.26 | 20.2 ± 0.7 | 430.4 ± 15.0 | 9.3 ± 0.3 |
| He I 4471.48 | 4476.09 ± 6.81 | 15.8 ± 17.3 | – | 6.1 ± 6.6 | 4472.00 ± 24.10 | 27.6 ± 69.5 | 7.8 ± 21.8 | 12.9 ± 36.4 | 4475.91 ± 26.52 | 20.7 ± 70.0 | 4.4 ± 15.4 | 8.4 ± 28.9 |
| | | | | | 4471.88 ± 0.29 | 27.6 ± 0.8 | 643.5 ± 21.9 | 13.0 ± 0.4 | 4475.85 ± 0.32 | 20.8 ± 0.8 | 371.1 ± 15.5 | 8.5 ± 0.4 |
| N III 4514.86 | 4517.31 ± 4.15 | 17.6 ± 10.7 | – | 12.2 ± 7.0 | 4515.72 ± 18.57 | 22.5 ± 49.5 | 9.7 ± 19.3 | 15.7 ± 31.3 | 4514.95 ± 18.61 | 21.5 ± 48.8 | 8.6 ± 17.7 | 15.3 ± 31.4 |
| | | | | | 4515.61 ± 0.23 | 22.4 ± 0.6 | 766.1 ± 19.3 | 15.7 ± 0.4 | 4514.86 ± 0.24 | 21.6 ± 0.6 | 690.9 ± 17.9 | 15.6 ± 0.4 |
| He II 4541.59 | 4544.26 ± 3.18 | 15.0 ± 8.2 | – | 12.6 ± 6.6 | 4544.30 ± 15.83 | 19.7 ± 39.5 | 9.5 ± 19.8 | 15.2 ± 31.5 | 4543.21 ± 14.87 | 19.3 ± 37.7 | 9.4 ± 18.5 | 16.1 ± 31.7 |
| | | | | | 4544.22 ± 0.21 | 19.8 ± 0.5 | 734.3 ± 19.9 | 15.2 ± 0.4 | 4543.16 ± 0.19 | 19.3 ± 0.5 | 720.5 ± 18.6 | 16.1 ± 0.4 |
| N V 4603.73 | 4607.31 ± 3.19 | 5.8 ± 7.7 | – | 2.8 ± 3.4 | 4607.39 ± 15.47 | 6.9 ± 37.4 | 1.4 ± 7.1 | 2.1 ± 10.5 | 4607.43 ± 16.80 | 8.2 ± 40.8 | 1.7 ± 7.9 | 2.6 ± 12.2 |
| | | | | | 4607.38 ± 0.22 | 6.9 ± 0.5 | 102.2 ± 7.1 | 2.1 ± 0.1 | 4607.43 ± 0.23 | 8.2 ± 0.6 | 122.4 ± 7.9 | 2.6 ± 0.2 |
| N III 4634.14, 4640.64 | 4641.70 ± 1.20 | 23.6 ± 3.0 | – | 61.6 ± 8.0 | 4640.92 ± 3.76 | 24.6 ± 9.6 | 40.0 ± 15.9 | 58.0 ± 23.1 | 4641.20 ± 3.65 | 25.0 ± 9.3 | 42.2 ± 16.0 | 63.8 ± 24.2 |
| | | | | | 4640.80 ± 0.05 | 24.6 ± 0.1 | 2766.0 ± 15.9 | 58.0 ± 0.3 | 4641.08 ± 0.05 | 25.0 ± 0.1 | 2922.6 ± 16.0 | 63.8 ± 0.3 |
| He II 4685.71 | 4688.22 ± 0.61 | 15.9 ± 1.6 | – | 67.0 ± 6.7 | 4687.77 ± 1.88 | 17.9 ± 5.0 | 49.5 ± 14.3 | 70.2 ± 20.3 | 4688.26 ± 1.78 | 17.7 ± 4.7 | 51.1 ± 14.0 | 74.9 ± 20.6 |
| | | | | | 4687.70 ± 0.03 | 17.9 ± 0.1 | 3259.2 ± 14.3 | 70.0 ± 0.3 | 4688.19 ± 0.03 | 17.7 ± 0.1 | 3357.5 ± 14.0 | 74.7 ± 0.3 |
| He II 4859.32 | 4862.82 ± 2.85 | 13.2 ± 7.1 | – | 13.4 ± 7.0 | 4862.77 ± 8.10 | 16.4 ± 20.6 | 10.2 ± 12.7 | 15.0 ± 18.8 | 4863.07 ± 7.62 | 16.1 ± 19.4 | 10.5 ± 12.6 | 15.5 ± 18.6 |
| | | | | | 4862.72 ± 0.15 | 16.5 ± 0.4 | 553.0 ± 12.7 | 15.0 ± 0.3 | 4863.02 ± 0.14 | 16.1 ± 0.4 | 568.5 ± 12.6 | 15.4 ± 0.3 |
| He II 5411.53 | 5414.87 ± 2.87 | 15.5 ± 7.3 | – | 19.6 ± 9.1 | 5415.18 ± 4.75 | 17.1 ± 12.1 | 18.4 ± 13.1 | 21.1 ± 15.0 | 5415.28 ± 4.58 | 17.3 ± 11.7 | 19.5 ± 13.3 | 22.6 ± 15.4 |
| | | | | | 5415.13 ± 0.15 | 17.1 ± 0.4 | 565.1 ± 13.1 | 21.0 ± 0.5 | 5415.23 ± 0.15 | 17.3 ± 0.4 | 598.8 ± 13.3 | 22.5 ± 0.5 |
| C IV 5801.33, 5811.98 | 5807.15 ± 5.34 | 22.1 ± 14.0 | – | 19.2 ± 12.9 | 5808.06 ± 7.06 | 24.0 ± 18.8 | 21.3 ± 18.2 | 22.1 ± 18.8 | 5808.51 ± 6.95 | 24.6 ± 18.5 | 22.5 ± 18.4 | 23.9 ± 19.5 |
| | | | | | 5807.97 ± 0.31 | 23.9 ± 0.8 | 475.2 ± 18.1 | 21.9 ± 0.8 | 5808.42 ± 0.31 | 24.5 ± 0.8 | 500.7 ± 18.3 | 23.7 ± 0.9 |
| He I 5875.62 | 5877.34 ± 4.84 | 21.5 ± 6.9 | – | 40.2 ± 28.5 | 5877.26 ± 6.20 | 22.2 ± 8.5 | 42.3 ± 47.8 | 38.9 ± 44.0 | 5877.58 ± 6.13 | 21.8 ± 8.3 | 40.6 ± 53.0 | 37.9 ± 49.4 |
| | | | | | 5877.20 ± 0.29 | 22.2 ± 0.4 | 895.2 ± 48.5 | 38.6 ± 2.1 | 5877.52 ± 0.29 | 21.8 ± 0.4 | 860.8 ± 53.7 | 37.6 ± 2.3 |
| He II 6527.10 | 6530.34 ± 15.56 | 10.8 ± 38.4 | – | 3.0 ± 10.0 | 6530.80 ± 17.81 | 12.6 ± 44.2 | 3.1 ± 10.5 | 3.0 ± 10.1 | 6531.23 ± 17.46 | 12.9 ± 43.3 | 3.3 ± 10.6 | 3.2 ± 10.3 |
| | | | | | 6530.79 ± 1.29 | 12.6 ± 3.2 | 42.8 ± 10.5 | 3.0 ± 0.7 | 6531.22 ± 1.27 | 12.9 ± 3.1 | 45.3 ± 10.6 | 3.2 ± 0.7 |
| He II 6560.10 | 6564.26 ± 3.44 | 20.2 ± 9.1 | – | 34.7 ± 16.4 | 6564.83 ± 3.20 | 22.0 ± 8.6 | 40.2 ± 16.9 | 38.1 ± 16.1 | 6565.19 ± 3.25 | 22.9 ± 8.9 | 42.5 ± 17.9 | 40.5 ± 17.0 |
| | | | | | 6564.78 ± 0.24 | 22.0 ± 0.6 | 543.7 ± 16.9 | 38.0 ± 1.2 | 6565.13 ± 0.24 | 22.9 ± 0.7 | 575.0 ± 17.8 | 40.4 ± 1.3 |
| He I+III 6683.00, 6683.20 | 6683.28 ± 9.34 | 31.0 ± 26.2 | – | 28.1 ± 28.2 | 6683.68 ± 8.55 | 31.9 ± 24.4 | 29.0 ± 26.8 | 27.8 ± 25.7 | 6684.21 ± 8.45 | 31.3 ± 23.9 | 28.4 ± 26.1 | 26.9 ± 24.7 |
| | | | | | 6683.58 ± 0.68 | 31.9 ± 1.9 | 366.4 ± 26.9 | 27.9 ± 2.0 | 6684.11 ± 0.67 | 31.3 ± 1.9 | 358.6 ± 26.1 | 27.0 ± 2.0 |
| He I 7065.19 | 7069.29 ± 13.50 | 29.4 ± 37.3 | – | 19.4 ± 26.7 | 7069.45 ± 11.81 | 31.7 ± 33.0 | 21.5 ± 24.6 | 20.7 ± 23.6 | 7070.03 ± 11.65 | 30.8 ± 32.3 | 20.6 ± 23.6 | 20.4 ± 23.3 |
| | | | | | 7069.35 ± 1.16 | 31.6 ± 3.2 | 219.0 ± 24.6 | 20.6 ± 2.3 | 7069.94 ± 1.14 | 30.8 ± 3.2 | 209.5 ± 23.5 | 20.3 ± 2.3 |
| N IV 7109.35, 7122.98 | 7118.34 ± 5.72 | 31.0 ± 15.1 | – | 48.7 ± 24.0 | 7119.19 ± 4.85 | 33.9 ± 12.9 | 57.2 ± 22.2 | 55.0 ± 21.3 | 7119.88 ± 4.70 | 34.0 ± 12.6 | 58.2 ± 22.1 | 57.9 ± 22.0 |
| | | | | | 7119.07 ± 0.49 | 33.9 ± 1.3 | 567.5 ± 22.2 | 54.8 ± 2.1 | 7119.77 ± 0.47 | 33.9 ± 1.3 | 575.9 ± 22.0 | 57.6 ± 2.2 |
| He II 7177.52 | 7182.91 ± 11.41 | 15.9 ± 29.9 | – | 8.3 ± 16.0 | 7181.31 ± 15.46 | 19.7 ± 42.0 | 7.0 ± 15.9 | 6.7 ± 15.3 | 7180.03 ± 16.67 | 21.8 ± 45.8 | 7.5 ± 17.4 | 7.6 ± 17.5 |
| | | | | | 7181.29 ± 1.61 | 19.7 ± 4.4 | 66.5 ± 15.9 | 6.6 ± 1.6 | 7180.02 ± 1.74 | 21.8 ± 4.8 | 72.0 ± 17.4 | 7.5 ± 1.8 |

2.2. WR classification

Visual spectral classification has been made using the emission line criteria introduced by [Smith et al. \(1996\)](#) for WN stars. The $\text{He II } \lambda 5411 / \text{He I } \lambda 5875$ flux ratio is about 0.82, which indicates the spectral subtype is WN7. It should be noted that the fluxes are based on Peak/Continuum values, and the absorption component is subtracted before measuring the Peak value of the $\text{He I } \lambda 5875$ emission line. The FWHM ($\text{He II } \lambda 4686$) of 17.0 \AA and $\text{EW}(\text{He II } \lambda 5411)$ of 21.4 \AA , indicate WR 121-16 is a narrow-line WR star. The $\lambda\lambda 4200, 4541,$ and 5411 are pure He II lines in the Pickering series, while $\lambda\lambda 4340$ and 4861 are Pickering lines that might be blended with $\text{H}\gamma$ and $\text{H}\beta$, respectively. Hydrogen will be detected, if the fluxes of $(\text{H} + \text{He}) \lambda\lambda 4340$ and 4861 lines clearly exceed those of the pure He II lines. Taking the Peak/Continuum flux for each line used in the calculation, $\lambda 4340 / \sqrt{\lambda 4200 \times \lambda 4541} - 1$ and $\lambda 4861 / \sqrt{\lambda 4541 \times \lambda 5411} - 1$ are -0.10 and -0.03 , respectively, indicates this star has no detectable hydrogen emission lines. Furthermore, the simultaneous presence of $\text{C IV } \lambda 5808$ and the even stronger $\text{N IV } \lambda 7109$ suggests that the star is in the transition phase between WN and WC stages ([Shara et al. 2016](#)). Hence this object can be classified as a WN7o/WC subtype star.

As shown in Fig. 5 of [Conti & Massey \(1989\)](#), WN/C transition stars are differentiated from WN stars in the diagram of the log of equivalent width of $\text{C IV } \lambda 5808$ versus $\text{He II } \lambda 4686$. This object has $\log \text{EW}(\text{He II } \lambda 4686) = 1.86$ and $\log \text{EW}(\text{C IV } \lambda 5808) = 1.33$, which are quite similar to those measured in the first WN/C star (1.83 and 1.38) found in M31 ([Shara et al. 2016](#)).

3. STELLAR PARAMETERS

3.1. Distance

The distance is necessary to derive absolute parameters such as luminosity, stellar mass and mass loss rate. Thanks to *Gaia*, parallaxes and proper motions are now available for 1.3 billion stars, which have been published in the second *Gaia* data release (GDR2, [Gaia Collaboration et al. 2018](#)). As discussed in [Bailer-Jones et al. \(2018\)](#) and [Luri et al. \(2018\)](#), the conversion of *Gaia* parallax ϖ to distance modifies the shape of the original parallax probability distribution, when the parallax error σ_ϖ is larger than $0.1 \times \varpi$. [Bailer-Jones et al. \(2018\)](#) have estimated distances of 1.3 billion stars from their parallaxes, with the help of a Bayesian approach. Using the distances given by this method, [Sander et al. \(2019\)](#) re-examined a previously studied sample of WC stars to derive key properties of the Galactic WC population. All quantities depending on the distance were updated, while the un-

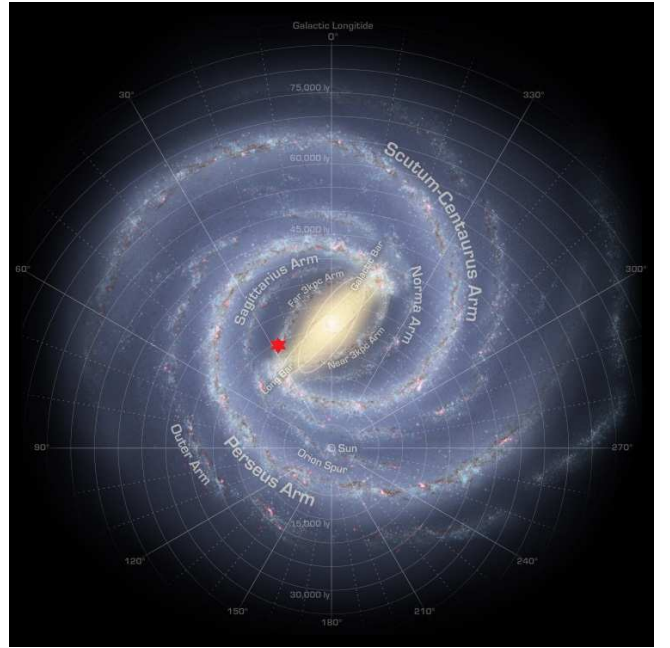


Figure 2. The position of WR 121-16 labeled as a red star in the Galactic Plane. The galactic coordinates are $(l, b) = (01^{\text{h}}51^{\text{m}}56^{\text{s}}.9, -02^{\circ}35'28''.0)$. This object is located in the Far 3kpc Arm. It is about 7.11 kpc from Earth, and 3.75 kpc from the Galactic Center. The background image is an artist's impression of the Milky Way, which shows the location of the spiral arms and the bulge. Background image credit: NASA/JPL-Caltech/ESO/R. Hurt

derlying spectral analyses remain untouched. A similar method has been applied to the Galactic WN population by [Hamann et al. \(2019\)](#). [Rate & Crowther \(2019\)](#) obtained distances of 383 Galactic WR stars from GDR2 parallaxes, using the Bayesian method with a prior based on H II regions and dust extinction. Distances agree with those from [Bailer-Jones et al. \(2018\)](#) for stars up to 2 kpc from the Sun, though deviate thereafter due to differing priors, leading to modest reductions in luminosities for recent WR spectroscopic results. The parallax of WR 121-16 has been measured in GDR2 as $\varpi = 0.01$ mas with a large error $\sigma_\varpi = 0.027$ mas. Hence, we can not derive the distance of the star by the simple inversion of $r = 1/\varpi$. Fortunately, the distance to this star was estimated by [Bailer-Jones et al. \(2018\)](#) as $r = 7.11_{-1.22}^{+1.56}$ kpc. We decide to use this value in the following analyses. It's found that this star is right located in the Far 3kpc Arm which was discovered by [Dame & Thaddeus \(2008\)](#). Besides, this star is about 3.75 kpc from the Galactic Center. The position of this WN/C star is marked as a red star in Figure 2.

3.2. PoWR model atmospheres

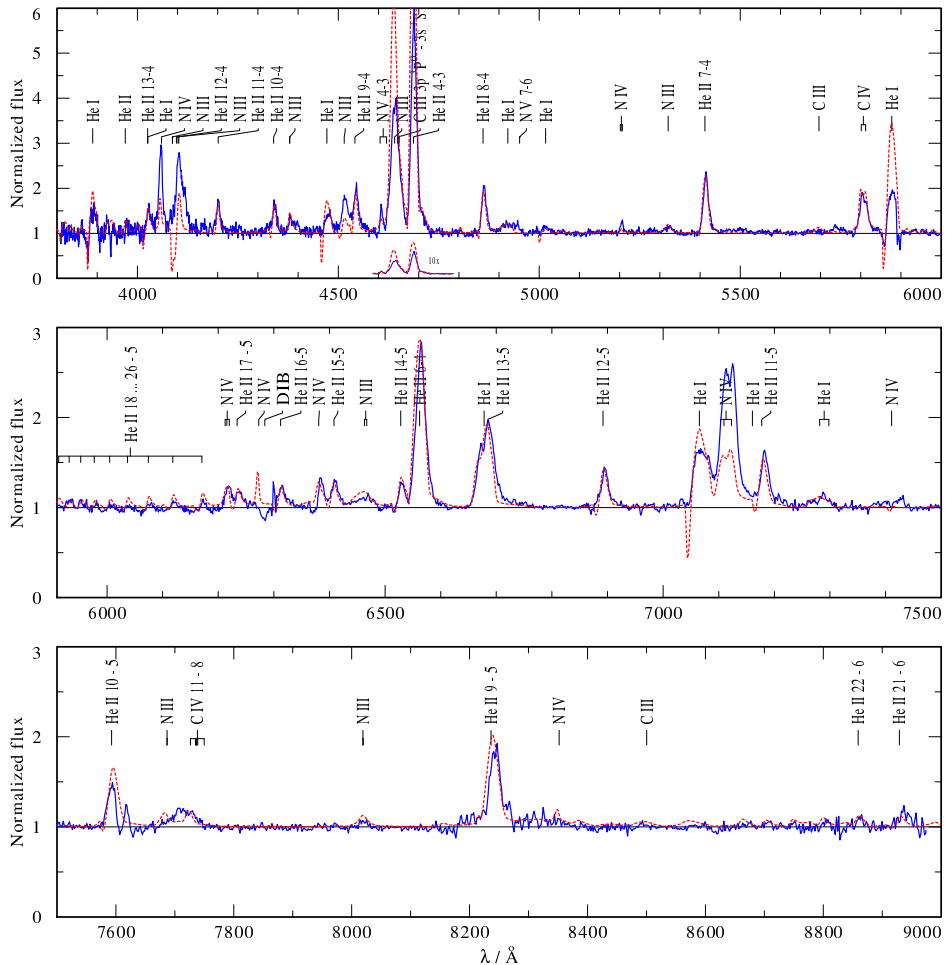


Figure 3. Spectral fitting with the PoWR synthetic spectrum. The blue line is the normalized LAMOST spectrum, while the red line is the synthetic spectrum.

The stellar parameters can be derived by comparing the observed spectra with the synthetic ones calculated from the Potsdam Wolf-Rayet (PoWR) model atmospheres, in which non-local thermal equilibrium (non-LTE), spherical expansion and metal line blanketing are considered. Some grids of models with fixed metallicity for WN stars (Hamann & Gräfener 2004; Todt et al. 2015) and WC stars (Sander et al. 2012) can be publicly obtained from the PoWR models website².

However, these models are not suitable for interpreting the transition WR stars. We changed the C, N, and O metallicity to generate a specific synthetic spectrum for this WN/C star. As the typical emission-line spectra of WR stars are predominantly formed by recombination processes in their dense stellar winds, the continuum-normalized spectrum shows a useful scale-invariance: for a given stellar temperature T_* , which we define at the stellar radius R_* ($\tau_{\text{Rosseland}} = 20$), and chemical compo-

sition, the equivalent widths of the emission lines depend only on the ratio between the volume emission measure of the wind and the area of the stellar surface, to a first approximation. An equivalent quantity, introduced by Schmutz et al. (1989), is the transformed radius

$$R_t = R_* \left(\frac{v_\infty}{2500 \text{ km s}^{-1}} \left/ \frac{\dot{M} \sqrt{D}}{10^{-4} M_\odot \text{ yr}^{-1}} \right. \right)^{2/3} \quad (1)$$

with the terminal velocity v_∞ and the microclumping parameter D , which is defined as the density contrast between wind clumps and a smooth wind of the same mass-loss rate. Hence, we fitted first the normalized LAMOST spectrum with this new PoWR spectrum by eye and show the results in Figure 3. In a second step, we fitted the synthetic spectral energy distribution to the observed flux-calibrated spectrum and photometry (Figure 4).

It appears difficult to achieve a good fit quality for all observed optical emission lines. The strongest lines N III $\lambda 4634$ - $\lambda 4640$ and He II $\lambda 4686$ can be best fitted with the

² <http://www.astro.physik.uni-potsdam.de/PoWR.html>

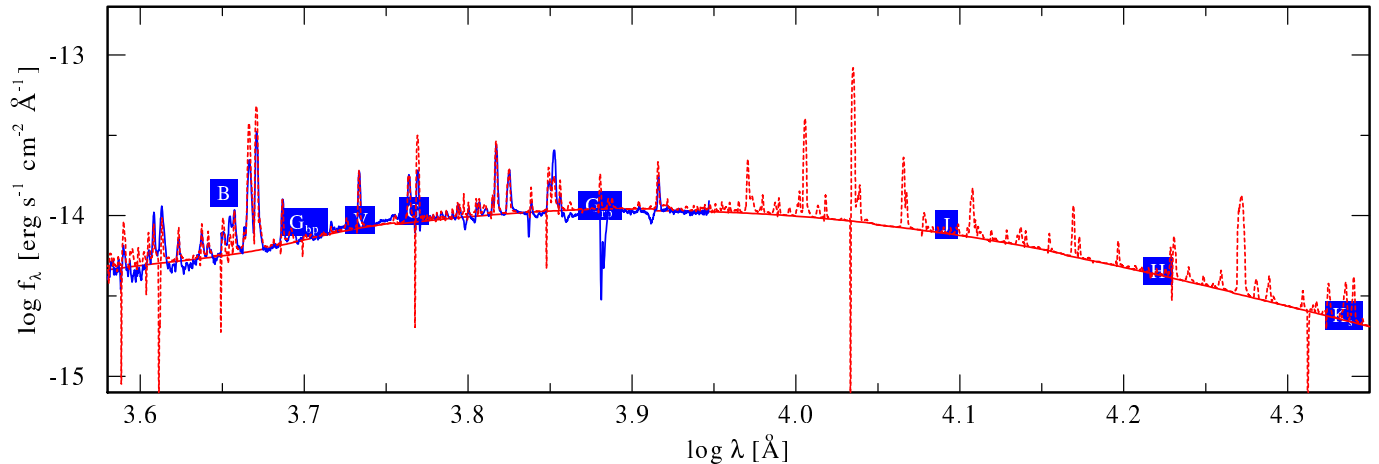


Figure 4. Deriving the reddening $E(B - V)$ by comparing the synthetic spectrum (red dotted line) with the flux-calibrated 2.16 m telescope spectrum (blue line) and with the observed *Gaia* and J, H, and K_s photometry. The continuum-only model flux (red line) is also shown for comparison.

Table 3. PoWR parameters of the new WN/C star.

| | | |
|----------------|---------------------------|-------------------------|
| T_* | kK | 47^{+9}_{-5} |
| $\log R_t$ | R_\odot | $0.8^{+0.2}_{-0.1}$ |
| v_∞ | km s^{-1} | 1000^{+200}_{-200} |
| $\log \dot{M}$ | $M_\odot \text{ yr}^{-1}$ | $-4.97^{+0.16}_{-0.20}$ |
| R_* | R_\odot | $4.14^{+1.4}_{-1.3}$ |
| $\log L$ | L_\odot | $4.88^{+0.17}_{-0.15}$ |
| M_* | M_\odot | $7.1^{+1.7}_{-1.1}$ |
| D | clumping factor | 4 |
| X_H | Mass fraction | 0.0% |
| X_{He} | Mass fraction | 98% |
| X_{Fe} | Mass fraction | 0.14% |
| X_N | Mass fraction | $1.5^{+1}_{-1}\%$ |
| X_C | Mass fraction | $0.2^{+0.1}_{-0.1}\%$ |
| X_O | Mass fraction | $<0.2\%$ |

stellar temperature $T_* = 42 \text{ kK}$ and the transformed radius $\log R_t/R_\odot = 1.0$, while the fit is worse for all other emission lines (see Figure 5). A better fit to the He I $\lambda 5876$ and the N IV lines can be obtained with a model that has $T_* = 56 \text{ kK}$ and $\log R_t/R_\odot = 0.7$ (see Figure 5). Our best compromise fit that gives a sufficient fit quality for almost all He II lines is therefore $T_* = 47^{+9}_{-5} \text{ kK}$ and $\log R_t/R_\odot = 0.8^{+0.2}_{-0.1}$.

Our compromise model fits all He II lines of the Pickering series well, therefore we infer $X_H = 0.0\%$ and $X_{He} = 98\%$. In the absence of a UV spectrum required to derive the abundance of the iron group elements, we adopted $X_{Fe} = 0.14\%$. The best fit to the emission lines of C III and C IV is for a carbon abundance of 0.2% (by mass), that is about 20 times the amount usually found in Galactic WNE and WNL stars (e.g.,

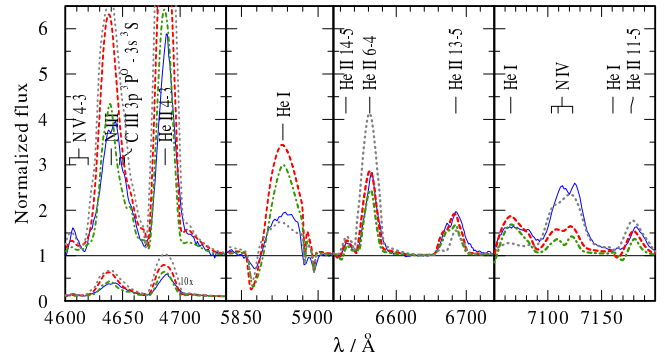


Figure 5. Details from the optical spectrum: Observation (blue solid line) and our compromise model (red dashed). Also shown is a model with $T_* = 42 \text{ kK}$ and $\log(R_t/R_\odot) = 1.0$ (green dashed-dotted) and a model with $T_* = 56 \text{ kK}$ and $\log(R_t/R_\odot) = 0.7$ (gray dotted). See text for details.

Hamann et al. 2006), but consistent with the value derived by Sander et al. (2012) for other Galactic WN/C stars, like WR 58 (0.1%) or WR 126 (5%). As there seems to be no prominent oxygen lines in the observations, we can only derive an upper limit of $X_O < 0.2\%$ from the absence of the O III $\lambda 5592$ line. We can not fit all the lines of N III, N IV, N V simultaneously with one set of stellar parameters, therefore it is harder to constrain the nitrogen abundance. However, most lines can be fitted with the typical value for WN stars of 1.5%, which is also found for WR 58.

We use the clumping factor $D = 4$, because a model for a homogeneous wind ($D = 1$) would result in too strong electron scattering line wings, and a higher value of $D = 10$ seems to underestimate the line wings. We use a so-called β -law to prescribe the velocity field $v(r) = v_\infty(1 - R_*/r)^\beta$ in the wind domain. The terminal velocity v_∞ is estimated from the widths of the emission

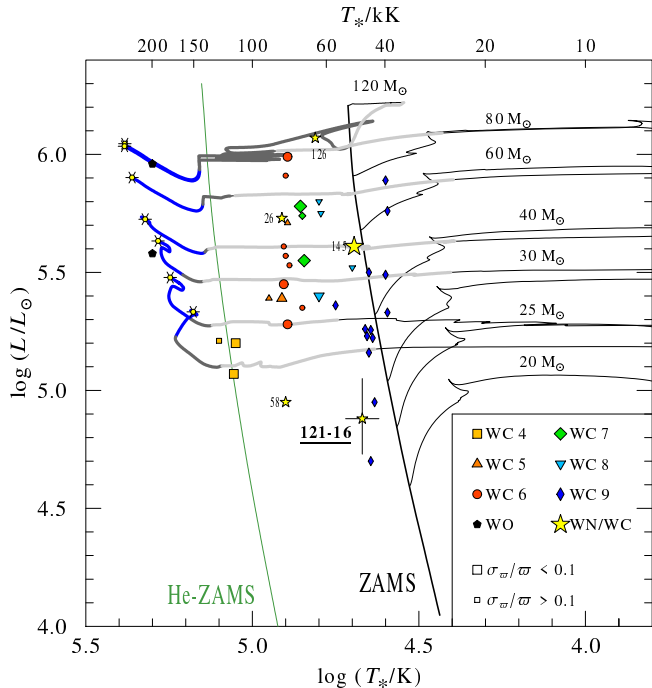


Figure 6. HRD with the WC, WO and WN/C star positions compared to the evolutionary tracks from Chieffi & Limongi (2013). WR 121-16 is plotted as a yellow star with error bars. The thick lines indicate the WR phases of the tracks. This figure is adapted from Sander et al. (2019).

lines, a value of 1000^{+200}_{-200} km s⁻¹ gives the best results. The best fit is achieved with $\beta = 1.0$, which is commonly used for other Galactic WR stars. However, the difficulties of fitting the helium and nitrogen lines of different ionization stages simultaneously might be resolved by a hydrodynamically consistent model, as demonstrated by Gräfener & Hamann (2005) for the WC star WR 111. A Doppler broadening of 100 km s⁻¹ was applied to all the spectral lines and gives a reasonable fit.

With the given *Gaia* parallax we fit our synthetic spectrum to the flux-calibrated spectrum from the 2.16 m telescope and to the observed *Gaia* and 2MASS (J, H, and K_s) photometry in Figure 4. The best fit is obtained for $\log L/L_{\odot} = 4.88$ and $E(B - V) = 1.20$ mag, using the extinction law by Fitzpatrick (1999). We note that the luminosity is quite low for a WR star, but WR 58 has also only a value of $\log L/L_{\odot} = 4.95$. With this luminosity the mass-loss rate is $\log \dot{M} = -4.97^{+0.16}_{-0.20}$ M_{\odot} yr⁻¹. The mass is estimated as about $7.1^{+1.7}_{-1.1}$ M_{\odot} based on the mass-luminosity relation for WN stars by Gräfener et al. (2011). A visual absolute magnitude $M_V = -3.955$ is inferred for WR 121-16 from its distance and reddening.

3.3. Comparison with evolutionary tracks

We show WR 121-16 and some WC, WO and four other WN/C stars in the Hertzsprung-Russell dia-

gram (HRD) in Figure 6. For comparison, the evolutionary tracks from Chieffi & Limongi (2013) obtained with the Frascati Raphson Newton Evolutionary Code (FRANEC) are also shown in the same figure. WR 121-16 is located in the “lower” luminosity regime. Even models with an initial equatorial rotational velocity of $v_{\text{rot, ini}} = 300$ km s⁻¹ can not reach the position of WR 121-16. We will not discuss this in detail as it is out of the scope of this paper.

4. IS IT A BINARY?

The observed binary frequency (including the probable binaries) of the Galactic WR stars is about 39% (van der Hucht 2001), and most of the binary companions are O-type stars. In WR+O binaries, the O-star’s contribution often dominates the overall composite spectrum (Sander et al. 2012). No signature of a possible O-type companion has been found in the spectrum of WR 121-16. Moreover, there is another possibility that this star is a WN+WC binary. However, there is no sign of radial velocity variation by comparing the emission lines in the LAMOST spectrum with those in the 2.16 m spectra. Therefore, the spectrum of WR 121-16 is probably not composited of a WN+WC binary, but rather a transition type WN/C star.

WR 121-16 has been collected in the American Association of Variable Star Observers (AAVSO) International Variable Star Index (VSX)³ with a name of ASASSN-V J185139.71-053451.1. The magnitude varies between 13.95 and 14.14 in *V*-band but no period has been found, and it was classified as Young Stellar Object (YSO) of unspecified variable type (Jayasinghe et al. 2018).

The Renormalised Unit Weight Error (RUWE) is expected to be around 1.0, if the astrometric observations of a source can be well fitted by the single-star model. The RUWE may be significantly greater than 1.0, if the source is non-single or there is problematic for the astrometric solution (Belokurov et al. 2020). Additionally, a positive excess noise could indicate the source deviates from the standard five-parameter astrometric model. For WR 121-16, $\text{RUWE} = 1.05$, $\text{astrometric_excess_noise} = 0.000$ mas and $\text{astrometric_excess_noise_sig} = 0.000$ provided by GDR2, indicate that this star is probably not a binary.

As a summary, the spectral and the time domain data, and the indices of the astrometric solution all support that WR 121-16 is probably a single star. Hence, the carbon and nitrogen emission lines are more likely from

³ www.aavso.org/vsx/

a WN/C single star, rather than a composite spectrum from a WN+WC binary.

5. SUMMARY

We have found a new Galactic WR star with coordinates of $(R.A., Dec)_{J2000} = (18^{\text{h}}51^{\text{m}}39^{\text{s}}.7, -05^{\circ}34'51''.1)$ in the LAMOST testing observations. According to the strong nitrogen and carbon emission lines simultaneously showing in the optical spectra, WR 121-16 can be classified as a transition WR of the WN7o/WC subtype. With the help of *Gaia* parallax, the distance from the Earth to WR 121-16 is inferred as $7.11_{-1.22}^{+1.56}$ kpc, and 3.75 kpc from the Galactic Center. Therefore, this object is located in the Far 3 kpc Arm.

By comparing the observed spectrum with the specific PoWR synthetic one, physical parameters with a stellar temperature of 47_{-5}^{+9} kK, a mass loss rate of $\dot{M} = 10^{-4.97_{-0.20}^{+0.16}} M_{\odot} \text{ yr}^{-1}$, and a stellar mass of $7.1_{-1.1}^{+1.7} M_{\odot}$ are derived. The carbon abundance is 0.2% by mass, which is about 20 times as high as that usually found in Galactic WN stars. The luminosity is as low as $\log L/L_{\odot} = 4.88_{-0.15}^{+0.17}$, that is similar to WR 58 which has a luminosity of $\log L/L_{\odot} = 4.95$. Besides, WR 121-16 is more likely a transition WN/C type, rather than a WN+WC binary.

ACKNOWLEDGMENTS

The authors thank the anonymous referee for helpful comments that improved this manuscript. W.Z. thanks Professor Paul Crowther for confirmation of the name of WR 121-16 for this star. This work is supported by the Joint Research Fund in Astronomy (No. U1531118) under cooperative agreement between the National Natural Science Foundation of China (NSFC) and Chinese Academy of Sciences (CAS). This work is also supported by the NSFC (No. 11733006) and the National Key R&D Program of China grant (No. 2017YFA0402704). C.-H. Hsia acknowledges the support from the Science and Technology Development Fund, MacauSAR (file no. 0007/2019/A) and Faculty Research Grants of the Macau University of Science and Technology (program no. FRG-19-004-SSI).

The Guoshoujing Telescope (the Large Sky Area Multi-Object Fiber Spectroscopic Telescope LAMOST) is a National Major Scientific Project built by the Chinese Academy of Sciences. Funding for the project has been provided by the National Development and Reform Commission. LAMOST is operated and managed by the National Astronomical Observatories, Chinese Academy of Sciences. We acknowledge the support of the staff of the Xinglong 2.16 m telescope. This work was partially supported by the Open Project Program of the Key Laboratory of Optical Astronomy, National Astronomical Observatories, Chinese Academy of Sciences.

REFERENCES

- Bailer-Jones, C. A. L., Rybizki, J., Fouesneau, M., Mantelet, G., & Andrae, R. 2018, *AJ*, 156, 58, doi: [10.3847/1538-3881/aacb21](https://doi.org/10.3847/1538-3881/aacb21)
- Belokurov, V., Penoyre, Z., Oh, S., et al. 2020, *MNRAS*, doi: [10.1093/mnras/staa1522](https://doi.org/10.1093/mnras/staa1522)
- Blanton, M. R., & Roweis, S. 2007, *AJ*, 133, 734, doi: [10.1086/510127](https://doi.org/10.1086/510127)
- Breysacher, J., Azzopardi, M., & Testor, G. 1999, *A&AS*, 137, 117, doi: [10.1051/aas:1999240](https://doi.org/10.1051/aas:1999240)
- Callingham, J. R., Tuthill, P. G., & Pope, B. J. S. a. 2019, *Nature Astronomy*, 3, 82, doi: [10.1038/s41550-018-0617-7](https://doi.org/10.1038/s41550-018-0617-7)
- Chieffi, A., & Limongi, M. 2013, *ApJ*, 764, 21, doi: [10.1088/0004-637X/764/1/21](https://doi.org/10.1088/0004-637X/764/1/21)
- Conti, P. S., & Massey, P. 1989, *ApJ*, 337, 251, doi: [10.1086/167101](https://doi.org/10.1086/167101)
- Crowther, P. A. 2007, *ARA&A*, 45, 177, doi: [10.1146/annurev.astro.45.051806.110615](https://doi.org/10.1146/annurev.astro.45.051806.110615)
- Crowther, P. A., De Marco, O., & Barlow, M. J. 1998, *MNRAS*, 296, 367, doi: [10.1046/j.1365-8711.1998.01360.x](https://doi.org/10.1046/j.1365-8711.1998.01360.x)
- Crowther, P. A., Drissen, L., Abbott, J. B., Royer, P., & Smartt, S. J. 2003, *A&A*, 404, 483, doi: [10.1051/0004-6361:20030503](https://doi.org/10.1051/0004-6361:20030503)
- Crowther, P. A., & Smith, L. J. 1996, *A&A*, 305, 541
- Crowther, P. A., Smith, L. J., & Willis, A. J. 1995, *A&A*, 304, 269
- Cui, X.-Q., Zhao, Y.-H., Chu, Y.-Q., et al. 2012, *Research in Astronomy and Astrophysics*, 12, 1197, doi: [10.1088/1674-4527/12/9/003](https://doi.org/10.1088/1674-4527/12/9/003)
- Dame, T. M., & Thaddeus, P. 2008, *ApJL*, 683, L143, doi: [10.1086/591669](https://doi.org/10.1086/591669)
- Fitzpatrick, E. L. 1999, *PASP*, 111, 63, doi: [10.1086/316293](https://doi.org/10.1086/316293)
- Frei, Z., & Gunn, J. E. 1994, *AJ*, 108, 1476, doi: [10.1086/117172](https://doi.org/10.1086/117172)
- Gaia Collaboration, Brown, A. G. A., Vallenari, A., et al. 2018, *A&A*, 616, A1, doi: [10.1051/0004-6361/201833051](https://doi.org/10.1051/0004-6361/201833051)
- Gómez-González, V. M. A., Mayya, Y. D., & Rosa-González, D. 2016, *MNRAS*, 460, 1555, doi: [10.1093/mnras/stw1118](https://doi.org/10.1093/mnras/stw1118)
- Gräfener, G., & Hamann, W. R. 2005, *A&A*, 432, 633, doi: [10.1051/0004-6361:20041732](https://doi.org/10.1051/0004-6361:20041732)
- Gräfener, G., Vink, J. S., de Koter, A., & Langer, N. 2011, *A&A*, 535, A56, doi: [10.1051/0004-6361/201116701](https://doi.org/10.1051/0004-6361/201116701)
- Hadfield, L. J., & Crowther, P. A. 2007, *MNRAS*, 381, 418, doi: [10.1111/j.1365-2966.2007.12284.x](https://doi.org/10.1111/j.1365-2966.2007.12284.x)
- Hamann, W. R., & Gräfener, G. 2004, *A&A*, 427, 697, doi: [10.1051/0004-6361:20040506](https://doi.org/10.1051/0004-6361:20040506)
- Hamann, W. R., Gräfener, G., & Liermann, A. 2006, *A&A*, 457, 1015, doi: [10.1051/0004-6361:20065052](https://doi.org/10.1051/0004-6361:20065052)
- Hamann, W. R., Gräfener, G., Liermann, A., et al. 2019, *A&A*, 625, A57, doi: [10.1051/0004-6361/201834850](https://doi.org/10.1051/0004-6361/201834850)
- Hillier, D. J. 1985, *AJ*, 90, 1514, doi: [10.1086/113864](https://doi.org/10.1086/113864)
- Hillier, D. J., Jones, T. J., & Hyland, A. R. 1983, *ApJ*, 271, 221, doi: [10.1086/161189](https://doi.org/10.1086/161189)
- Jarrett, T. H., Cohen, M., Masci, F., et al. 2011, *ApJ*, 735, 112, doi: [10.1088/0004-637X/735/2/112](https://doi.org/10.1088/0004-637X/735/2/112)
- Jayasinghe, T., Kochanek, C. S., Stanek, K. Z., et al. 2018, *MNRAS*, 477, 3145, doi: [10.1093/mnras/sty838](https://doi.org/10.1093/mnras/sty838)
- Luo, A. L., Zhao, Y.-H., Zhao, G., et al. 2015, *Research in Astronomy and Astrophysics*, 15, 1095, doi: [10.1088/1674-4527/15/8/002](https://doi.org/10.1088/1674-4527/15/8/002)
- Luri, X., Brown, A. G. A., Sarro, L. M., et al. 2018, *A&A*, 616, A9, doi: [10.1051/0004-6361/201832964](https://doi.org/10.1051/0004-6361/201832964)
- Massey, P., & Grove, K. 1989, *ApJ*, 344, 870, doi: [10.1086/167854](https://doi.org/10.1086/167854)
- Massey, P., Neugent, K. F., Morrell, N., & Hillier, D. J. 2014, *ApJ*, 788, 83, doi: [10.1088/0004-637X/788/1/83](https://doi.org/10.1088/0004-637X/788/1/83)
- Morgan, D. H., & Good, A. R. 1987, *MNRAS*, 224, 435, doi: [10.1093/mnras/224.2.435](https://doi.org/10.1093/mnras/224.2.435)
- Rate, G., & Crowther, P. A. 2019, in *The Gaia Universe*, 45, doi: [10.5281/zenodo.3233991](https://doi.org/10.5281/zenodo.3233991)
- Roman-Lopes, A., Román-Zúñiga, C. G., Borissova, J., et al. 2020, *ApJ*, 891, 107, doi: [10.3847/1538-4357/ab72a6](https://doi.org/10.3847/1538-4357/ab72a6)
- Rosslowe, C. K., & Crowther, P. A. 2015a, *MNRAS*, 449, 2436, doi: [10.1093/mnras/stv502](https://doi.org/10.1093/mnras/stv502)
- . 2015b, *MNRAS*, 447, 2322, doi: [10.1093/mnras/stu2525](https://doi.org/10.1093/mnras/stu2525)
- Sander, A., Hamann, W. R., & Todt, H. 2012, *A&A*, 540, A144, doi: [10.1051/0004-6361/201117830](https://doi.org/10.1051/0004-6361/201117830)
- Sander, A. A. C., Hamann, W. R., Todt, H., et al. 2019, *A&A*, 621, A92, doi: [10.1051/0004-6361/201833712](https://doi.org/10.1051/0004-6361/201833712)
- Schild, H., Smith, L. J., & Willis, A. J. 1990, *A&A*, 237, 169
- Schmutz, W., Hamann, W. R., & Wessolowski, U. 1989, *A&A*, 210, 236
- Shara, M. M., Mikołajewska, J., Caldwell, N., et al. 2016, *MNRAS*, 455, 3453, doi: [10.1093/mnras/stv2455](https://doi.org/10.1093/mnras/stv2455)
- Smith, L. F. 1968, *MNRAS*, 138, 109, doi: [10.1093/mnras/138.1.109](https://doi.org/10.1093/mnras/138.1.109)
- Smith, L. F., Shara, M. M., & Moffat, A. F. J. 1990, *ApJ*, 358, 229, doi: [10.1086/168978](https://doi.org/10.1086/168978)
- . 1996, *MNRAS*, 281, 163, doi: [10.1093/mnras/281.1.163](https://doi.org/10.1093/mnras/281.1.163)
- Smith, L. J., Crowther, P. A., & Prinja, R. K. 1994, *A&A*, 281, 833
- Su, D.-Q., & Cui, X.-Q. 2004, *ChJA&A*, 4, 1, doi: [10.1088/1009-9271/4/1/1](https://doi.org/10.1088/1009-9271/4/1/1)
- Todt, H., Sander, A., Hainich, R., et al. 2015, *A&A*, 579, A75, doi: [10.1051/0004-6361/201526253](https://doi.org/10.1051/0004-6361/201526253)

van der Hucht, K. A. 2001, *NewAR*, 45, 135,
doi: [10.1016/S1387-6473\(00\)00112-3](https://doi.org/10.1016/S1387-6473(00)00112-3)

Wang, S.-G., Su, D.-Q., Chu, Y.-Q., Cui, X., & Wang,
Y.-N. 1996, *ApOpt*, 35, 5155, doi: [10.1364/AO.35.005155](https://doi.org/10.1364/AO.35.005155)

Zhao, G., Zhao, Y.-H., Chu, Y.-Q., Jing, Y.-P., & Deng,
L.-C. 2012, *Research in Astronomy and Astrophysics*, 12,
723, doi: [10.1088/1674-4527/12/7/002](https://doi.org/10.1088/1674-4527/12/7/002)

Zhao, Y., Fan, Z., Ren, J.-J., et al. 2018, *Research in
Astronomy and Astrophysics*, 18, 110,
doi: [10.1088/1674-4527/18/9/110](https://doi.org/10.1088/1674-4527/18/9/110)